ChemComm

Accepted Manuscript

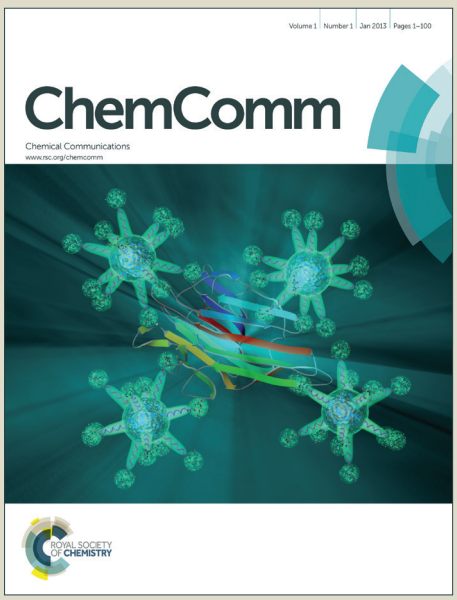

ROYAL SOCIETY OF CHEMISTRY

www.rsc.org/chemcomm

ChemComm

RSCPublishing

COMMUNICATION

Mn^{II}-containing coordination nanoparticles as highly efficient T_1 contrast agents for Magnetic Resonance Imaging

Cite this: DOI: 10.1039/x0xx00000x

Received 00th January 2014,
Accepted 00th January 2014

DOI: 10.1039/x0xx00000x

www.rsc.org/

Gabriella Paul,[a] Yoann Prado,[a] Nada Dia,[a,b] Eric Rivière,[a] Sophie Laurent,[c] Mathieu Roch,[d] Luce Vander Elst,[c,d] Robert N. Muller,[c,d] Lucie Sancey,[e] Pascal Perriat,[f] Olivier Tillement,[e] Talal Mallah[a] and Laure Catala[a]*

Large longitudinal relaxivities were observed in Mn^{II}-containing Prussian blue analogues nanoparticles. At low concentration and high field (7T), a remarkable positive contrast enhancement was seen which exceeded that of clinical contrast agents and was attributed to the very large proportion of surface atoms of these coordination nanoparticles.

Magnetic Resonance Imaging (MRI) is a non-invasive technique that allows the diagnosis of diseaded zones. In 30% of clinical tests contrast agents (CAs) are used to enhance image quality. Designing positive CAs denoted as T_1-CAs with larger longitudinal relaxivities (r_1) is one manner to reduce the injected dose into the patient. The brightening conferred by such CAs originates from the fast proton relaxation of water molecules coordinated to paramagnetic ions with a large spin, a long electronic relaxation time and fast water exchange rate such as in Gd^{III} chelates commonly used as clinical CAs and in Mn^{II} complexes.[1-3] One valuable strategy to improve their efficiency and delay their blood clearance is to use larger structures including these paramagnetic complexes or ions. A longer rotational correlation time leading to an enhanced longitudinal relaxivity are the result of slow tumbling due to the high molecular weight of the nano-object.[1,2] This has been reported for Gd^{III} and Mn^{II} complexes grafted on polymers, particles, proteins and in liposomes.[1-11] Nevertheless, in general local reorientation of the complexes leads to low values of relaxivities. Hence, active paramagnetic species directly included into the NPs' core is a way to circumvent this problem as described for some Gd^{III} and Mn^{II} oxides[7-8,12-17], fluorides[18] and metal organic frameworks.[19-25] Among microporous networks, cyano-bridged coordination networks such as Prussian blue analogues (PBA) NPs have been extensively investigated for their magnetic/electronic properties[26-29] but less focus has been placed on MRI-CAs, despite the FDA approval of Prussian blue. Citrate coated Prussian blue NPs of 13 nm have been reported[30,31] with a modest negative (T_2) contrast enhancement, while Gd^{III}-containing polycyanometallate NPs below 5 nm coated with polysaccharides (either in acidic[32] or neutral[33,34] aqueous media) and PB NPs containing Gd^{III} [35] structures around 100 nm revealed high longitudinal relaxivities. Recently large Mn^{II} PBA particles have been reported (on exchange resin or with silica) with large transverse relaxivities ($100<r_2<205$ $mM^{-1}.s^{-1}$) that are adapted to T_2-weighted images.[36]

In this communication, $K_{4y-3+x}Mn^{II}_xIn^{III}_{1-x}[Fe^{II}(CN)_6]_y$ NPs with controlled contents in Mn^{II} have been obtained between 5 and 21 nm through coprecipitation by a one-step process in water without any additional reactant, followed by post-coating by Dextran. These new compounds (abbreviated as MnInFe@Dextran NPs) exhibit large longitudinal relaxivities for Mn^{II}-based CAs (and r_2/r_1 close to 2) that exceed those of Mn^{II} oxide NPs. A remarkable positive T_1 contrast enhancement was registered overtaking that of clinical chelate Gd-DTPA (Magnevist) in conditions usually unfavorable to T_1 paramagnetic oxide NPs, ie at low paramagnetic ion concentration (0.2 mM of Mn^{II}) under high field (7T) and with short TR MRI sequence.

Nanoparticles were produced without any additive by fast mixing of an aqueous solution of hexacyanoferrate(II) with an aqueous solution containing Mn^{II} and In^{III} salts in variable ratios x= $[Mn^{II}]/[In^{III}]$ from x = 0.05 to x = 0.9 (see SI).

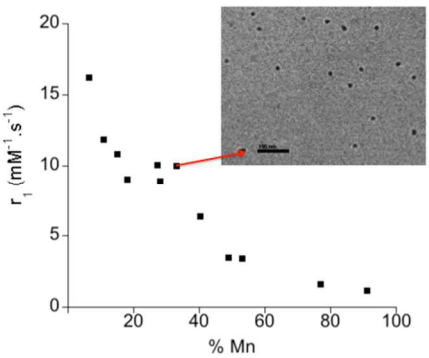

Fig. 1. Longitudinal relaxivity r_1 dependence of MnInFe@Dextran NPs with different Mn^{II} ion contents. Insert: TEM image of NP-33%.

Formation of stable colloidal solutions without aggregation was monitored by Dynamic Light Scattering (DLS) and reveal hydrodynamic diameters that depend on the Mn^{II} ions content for x>0.4 (Fig. S1). Without the introduction of In^{III} ions (x=1), the colloidal solution is unstable. Introduction of only 10% of In^{III} ions enables the control NPs below 20 nm while 90 % of In^{III} ions leads to a hydrodynamic diameter of 7 nm. This is related to the high insolubility of InFe PBA that controls the nucleation rate. Powders of NPs obtained with 0.05<x<0.9 were recovered by adding 25 equivalents of Dextran monomer per ferrocyanide and flocculation with acetone. MnInFe@Dextran NPs were subsequently dispersed in water up to 10 mM with a stability over a period of months without any change in hydrodynamic diameter. Transmission Electron Microscopy (TEM) was carried out on these dispersions and revealed homogeneous nanoparticles isolated by Dextran chains, with an average size ranging from 4±1 nm to 20.7±3.5 nm for x= 0.05 and x=0.9 respectively (Fig. 1 insert and S2). X-Ray powder diffraction performed on the powders has confirmed the face centered cubic structure of the NPs in all samples (Fig. S3), with a decrease of the average cell parameter from 10.43 Å to 10.13 Å as the Mn^{II} ion content raised from x=0.05 to x=0.9, in good agreement with the smaller ionic radius of Mn^{II} ion compared to In^{III} ion. This indicates that Mn^{II} ions do insert in the coordination network. Fourier Transform Infra-red (FT-IR) spectra recorded on the different compounds revealed a broad band with two contributions at 2067 cm^{-1} and 2108 cm^{-1} that were attributed to the superimposed asymmetric vibrations of the bridged cyanides Mn^{II}-NC-Fe^{II} and In^{III}-NC-Fe^{II}, respectively, with the most intense contributions shifted to low frequencies for larger Mn^{II} proportions (Fig. S4). The composition of metal ions and Dextran was assessed by elemental analysis (Fig. S5) that showed a decrease of the ferrocyanide vacancies from 20% to 10% when decreasing x. It is possible to estimate the number of Dextran chains (~100) from the size and composition considering an average degree of polymerization of 247, leading to around 3 anchoring points between each chain and the NPs' surface. Magnetic measurements recorded at 5 K (Fig. S6) confirmed the paramagnetic behaviour of all samples, with a coherent increase of the magnetization value at 5T as the Mn^{II} contents increase (the other ions In^{III} and low spin Fe^{II} are diamagnetic). Relaxometry measurements were registered at 37°C (310 K) under a field of 1.5 T on the colloidal solutions obtained on samples with 0.05<x<0.9 (Fig. 1). The longitudinal and transverse relaxivities r_i (i=1,2 respectively) expressed per mM of Mn^{II} ion (the other ions being diamagnetic) show a strong dependence on the Mn^{II} content meaning that all Mn^{II} ions are not equivalent depending on their location at the surface or in the core of the particles. Large longitudinal relaxivities between r_1 = 9 $mM^{-1}.s^{-1}$ up to r_1 = 15 $mM^{-1}.s^{-1}$ have been determined for samples with x = 0.3 to x = 0.05 respectively. A value of r_1 = 15 $mM^{-1}.s^{-1}$ per Mn^{II} ion is 40 times that of 7 nm MnO nanoparticles[15] and about twice that reported for the best 2.5 nm MnO nanoparticles[7,8] (also recorded at 1.5 T). Since in this range of Mn^{II} content the particles' size is around 5 nm, the high proportion of Mn^{II} ions located at the particles' surface (calculated around 45 %, Fig S7) may explain this efficiency as these ions have a larger number of coordinated water molecules in efficient exchange with bulk water.[¶] When increasing the Mn^{II} proportion from x=0.4 to x=0.9, the r_1 values decrease from 5 $mM^{-1}.s^{-1}$ to 1.6 $mM^{-1}.s^{-1}$ (expressed per mM of Mn^{II} ions). In this range of Mn^{II} content, particles' size increases together with the Mn^{II} content resulting in (i) a decrease of the relative quantity of ions located at the nanoparticles surface and (ii) an increasing number of Mn^{II} ions located in the core of the particles and thus less active on the proton relaxation. The transverse relaxivities r_2 follow the same trend as for r_1 with values comprised between 30 $mM^{-1}.s^{-1}$ and 1.4 $mM^{-1}.s^{-1}$ (per mM of Mn^{II} ions), and r_2/r_1 ratios between 1.1 and 1.8 that confirm these particles are expected to behave as positive CAs (Fig. S8). These measurements were reproduced on different batches of particles.

Among the various samples, nanoparticles with a proportion of 33% Mn (x=0.33 denoted as NP-33%) were selected as they display the best relaxivity for the minimum total amount of metallic ions of Fe^{II}, In^{III} and Mn^{II} (see calculation in S9). The nuclear magnetic relaxation dispersion (NMRD) profile of NP-33% at 37°C shows a typical frequency dependence of r_1 for slow tumbling CAs that confirm Mn^{II} ions are incorporated in the NPs' cores (Fig. 2a). In addition, the low frequency profile discards any free Mn^{II} ion. The decrease of longitudinal relaxivity r_1 at 300 MHz (7T) is similar to that usually observed for paramagnetic nanoparticles. Longitudinal relaxivity was also registered at 60 MHz (3 T) at 5 °C and increases from r_1 = 10.0 $mM^{-1}.s^{-1}$ at 37 °C to 12.9 $mM^{-1}.s^{-1}$ at 5°C (Fig. S10), suggesting that the water exchange is not the limiting parameter but rather the rotational correlation time. In addition, the filtrate obtained after ultrafiltration of the colloidal solution was analyzed: its relaxation time is that of water and ICP measurement reveals negligible Mn^{II} and In^{III} content (4 µg/L for Mn^{II}, i.e. 75 nM corresponding to 0.4 % of the initial concentration and below the detection threshold for In^{III}, *i.e.* less than 2 % of the initial concentration), that confirms the high stability of these nano-objects. This is further supported by a constant value of the longitudinal relaxation time T_1 recorded on the stable colloidal solution after 6 months and by DLS measurement recorded in serum at 5 mM (Fig. S11).

Importantly, a large T_1–weighted contrast enhancement was observed for NP-33% under a 7 T field (300 MHz) at a concentration of 0.2 mM in Mn^{II} ions overcoming that of GdDTPA (Fig. 2b). The high contrast observed at high field and low concentration may be further increased if recorded at 3 T (60 MHz). This highlights the remarkable activity as a T_1-CA compared to Mn^{II}-based oxides (that are usually compared to pure water). This efficiency can be related to a moderate r_2 (and thus low r_2/r_1) due to a weak number of paramagnetic sites contained in these 5 nm NPs (only 240 Mn^{II} atoms per particle, since In^{III} and Fe^{II} are diamagnetic) combined to the efficient exchange of water on the Mn^{II} atoms located at the NPs periphery. Indeed, the presence of Dextran does not impede the exchange of water molecules as the "bare" NP-33% have a smaller relaxivity (r_1 = 7 $mM^{-1}.s^{-1}$ at 37°C and 1.5 T) compared to coating NP-33%, due to the decrease of the rotational correlation time. This again suggests that the former is the parameter limiting the relaxivity for these nanosystems.

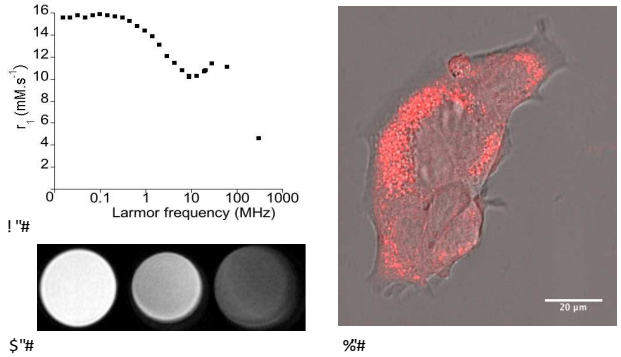

Fig. 2. a) NMRD profile on NP-33% at 37°C b) T_1-weighted MR image for left: NP-33% at [Mn^{II}] = 0.2 mM, center: Gd-DTPA clinical CA at [Gd^{III}] = 0.2 mM and right: water, from a 7T clinical MRI system with a spin gradient sequence with TR = 22 ms and

TE= 3 ms. c) Cell internalization of NP-33% coated by Dextran-TRITC after 60 min.

Cytotoxicity of NP-33% was examined with the MTT test performed on two cell lines. The HEK293 cells were unaffected after 24 h below concentrations of 5 mM of NP-33% and comparable to pure Dextran (no toxicity at 8 mg/mL, Fig. S12). Murin mammal cells revealed an IC_{50} of 3.8 mg/mL (532 μM of NP-33%) after 24 h, while it remained non-toxic for short times (1h) up to 19 mg/mL (2 mM, Fig. S12). In summary, NP-33% are observed to be non-toxic to weakly toxic up to fairly high concentrations for short and long times respectively, and appears to be dependent on the cell line. *In vitro* studies have been performed also to monitor cell internalization by confocal microscopy at λ= 550−700 nm using NP-33% coated with Dextran chains labeled with 0.1% of the fluorescent tetramethylrhodamine (TRITC) (Fig. S13) and fully characterized as the unlabelled ones (Fig. S14). Fast internalization in less than 30 min has been observed with the formation of vesicles (Fig. 2c and S15) and no penetration detected in the cell nucleus.

Conclusions

In summary, the high proportion of atoms located at surface of these nanoparticles as compared to oxide or metal nanoparticles due to the low metallic density of microporous PBAs leads to remarkable longitudinal relaxivities per Mn^{II} atom among the largest reported for Mn^{II} with that of Si quantum dots clusters doped with Mn^{II}.[37] As a consequence of a low r_2/r_1 ratio, a large T_1-contrast enhancement is registered at low concentrations of Mn^{II} ions under high field conditions and short MRI sequence overcoming that of Gd-based clinical CAs. Their high stability, low toxicity and water-based preparation at room temperature makes this family of Mn^{II}-based PBA contrast agents promising candidates for *in vivo* MRI diagnosis. Incorporation of ^{111}In and other active probes for Single Photon Emission Computed Tomography (SPECT) will lead to confer multimodality to these new CAs.[38]

Aknowledgments
Authors thank the Center for Microscopy and Molecular Imaging (CMMI, supported by the European Regional Development Fund and the Walloon Region). This work was supported by Walloon Region (program First spin-off), FNRS (Fond National de la Recherche Scientifique), UIAP VII and ARC Programs of the french Community of Belgium, BELSPO, COST Actions (D38 and TD1004), the EMIL program, the French CNRS, the Université Paris Sud, the Institut Universitaire de France, the Lebanese CNRS and the Université Libanaise for their financial support. We thank Philippe Mejanelle for ICP measurement.

Notes and references

[a] Institut de Chimie Moléculaire et des Matériaux d'Orsay, CNRS, Université Paris 11, 91405 Orsay, France. Fax: +33169154754; Tel+33169157890; E-mail: laure.catala@u-psud.fr

[b] Ecole Doctorale des Sciences et de Technologie, Hadath campus P.O.Box 5, Université Libanaise Beyrouth, Liban

[c] Univ Mons, NMR & Mol Imaging Lab, Dept Gen Organ & Biomed Chem, B-7000 Mons, Belgium.

[d] CMMI : Center for Microscopy and Molecular Imaging, Rue Adrienne Bolland, 8, B-6041 Gosselies, Belgium.

[e] Institut Lumière Matière Equipe FENNEC - UMR CNRS 5306 - Univ. Lyon 1Bâtiment Jules Raulin, 2, rue V. Grignard 69622 Villeurbanne

[f] INSA Lyon, 7, Avenue Jean Capelle, 69621 Villeurbanne.

¶Because of less than 10% ferrocyanide vacancies in this range of Mn^{II} contents and albeit the microporosity of the network, internal Mn^{II} ions that bear a small number of water molecules are not expected to play a relevant role in these compounds.

Electronic Supplementary Information (ESI) available: [Synthetic procedure and all detailed XRD, DLS, IR, elemental analysis TEM]. See DOI: 10.1039/c000000x/

1. Caravan, P.; Ellison, J. J.; McMurry, T. J.; Lauffer, R. B., *Chem Rev* **1999**, 99, 2293-2352.
2. Lauffer, R. B., *Chem Rev* **1987**, 87, 901-927.
3. Drahos, B.; Lukes, I.; Toth, E., *Eur J Inorg Chem* **2012**, 1975-1986.
4. Laurent, S.; Henoumont, C.; Vander Elst, L.; Muller, R. N., *Eur J Inorg Chem* **2012**, 1889-1915.
5. Aime, S.; Castelli, D. D.; Lawson, D.; Terreno, E., *J Am Chem Soc* **2007**, 129, 2430-2431.
6. Tóth, E.; Bolskar, R. D.; Borel, A.; Gonzalez, G.; Helm, L.; Merbach, A. E.; Sitharaman, B.; Wilson, L. J., *J Am Chem Soc* **2005,** *127*, 799-805
7. Kueny-Stotz, M.; Garofalo, A.; Felder-Flesch, D., *Eur J Inorg Chem* **2012**, 1987-2005.
8. Zhen, Z. P.; Xie, J., *Theranostics* **2012**, 2, 45-54
9. Alric, C.; Taleb, J.; Le Duc, G.; Mandon, C.; Billotey, C.; Le Meur-Herland, A.; Brochard, T.; Vocanson, F.; Janier, M.; Perriat, P.; Roux, S.; Tillement, O., *J Am Chem Soc* 2008, 130, 5908-5915.
10. Moriggi, L.; Cannizzo, C.; Dumas, E.; Mayer, C. R.; Ulianov, A.; Helm, L., *J Am Chem Soc* **2009,** *131*, 10828-10829.
11. Ferreira, M. F.; Mousavi, B.; Ferreira, P. M.; Martins, C. I. O.; Helm, L.; Martins, J. A.; Geraldes, C. F. G. C., *Dalton Trans* **2012,** *41*, 5472-5475
12. Bridot, J. L.; Faure, A. C.; Laurent, S.; Rivière, C.; Billotey, C.; Hiba, B.; Janier, M.; Josserand, V.; Coll, J. L.; Vander Elst, L.; Muller, R.; Roux, S.; Perriat, P.; Tillement, O., *J Am Chem Soc* **2007**, 129, 5076-5084.
13. Kim, T.; Momin, E.; Choi, J.; Yuan, K.; Zaidi, H.; Kim, J.; Park, M.; Lee, N.; McMahon, M. T.; Quinones-Hinojosa, A.; Bulte, J. W. M.; Hyeon, T.; Gilad, A. A., *J Am Chem Soc* **2011**, 133, 2955-2961.
14. Na, H. B.; Hyeon, T., *J Mater Chem* **2009**, 19, 6267-6273.
15. Na, H. B.; Lee, J. H.; An, K. J.; Park, Y. I.; Park, M.; Lee, I. S.; Nam, D. H.; Kim, S. T.; Kim, S. H.; Kim, S. W.; Lim, K. H.; Kim, K. S.; Kim, S. O.; Hyeon, T., *Angew Chem Int Edit* **2007**, 46, 5397-5401.
16. Yu, T.; Moon, J.; Park, J.; Park, Y. I.; Bin Na, H.; Kim, B. H.; Song, I. C.; Moon, W. K.; Hyeon, T., *Chem Mater* **2009**, 21, 2272-2279.
17. Shukoor, M. I.; Natalio, F.; Tahir, M. N.; Wiens, M.; Tarantola, M.; Therese, H. A.; Barz, M.; Weber, S.; Terekhov, M.; Schroder, H. C.; Muller, W. E. G.; Janshoff, A.; Theato, P.; Zentel, R.; Schreiber, L. M.; Tremel, W., *Adv Funct Mater* **2009**, 19, 3717-3725.
18. Johnson, N. J. J.; Oakden, W.; Stanisz, G. J.; Prosser, R. S.; van Veggel, F. C. J. M., *Chem Mater* **2011**, 23, 4877-4877.
19. Rieter, W. J.; Taylor, K. M. L.; An, H. Y.; Lin, W. L.; Lin, W. B., *J Am Chem Soc* **2006,** *128*, 9024-9025.
20. Taylor, K. M. L.; Rieter, W. J.; Lin, W. B., *J Am Chem Soc* **2008,** *130*, 14358-14359.
21. Taylor-Pashow, K. M. L.; Della Rocca, J.; Xie, Z. G.; Tran, S.; Lin, W. B., *J Am Chem Soc* **2009**, 131, 14261-14261.
22. Horcajada, P.; Chalati, T.; Serre, C.; Gillet, B.; Sebrie, C.; Baati, T.; Eubank, J. F.; Heurtaux, D.; Clayette, P.; Kreuz, C.; Chang, J. S.; Hwang, Y. K.; Marsaud, V.; Bories, P. N.; Cynober, L.; Gil, S.; Ferey, G.; Couvreur, P.; Gref, R., *Nat Mater* **2010**, 9, 172-178.
23. Horcajada, P.; Gref, R.; Baati, T.; Allan, P. K.; Maurin, G.; Couvreur, P.; Ferey, G.; Morris, R. E.; Serre, C., *Chem Rev* **2012**, 112, 1232-1268
24. Cunha, D.; Ben Yahia, M.; Hall, S.; Miller, S. R.; Chevreau, H.; Elkaim, E.; Maurin, G.; Horcajada, P.; Serre, C., *Chem Mater* **2013**, 25, 2767-2776.
25. Carne-Sanchez, A.; Bonnet, C. S.; Imaz, I.; Lorenzo, J.; Tóth, E.; Maspoch, D., *J Am Chem Soc* **2013,** *135*, 17711-17714
26. Catala, L.; Volatron, F.; Brinzei, D.; Mallah, T., *Inorg Chem* **2009,** *48*, 3360-3370.
27. Catala, L.; Gloter, A.; Stephan, O.; Rogez, G.; Mallah, T., *Chem Commun* **2006**, 1018-1020.
28. Galvez, N.; Sanchez, P.; Dominguez-Vera, J. M., *Dalton Trans* **2005**, 2492-2494.

29. Larionova, J.; Guari, Y.; Sangregorio, C.; Guerina, C., *New J Chem* **2009,** *33*, 1177-1190.
30. Shokouhimehr, M.; Soehnlen, E. S.; Hao, J. H.; Griswold, M.; Flask, C.; Fan, X. D.; Basilion, J. P.; Basu, S.; Huang, S. P. D., *J Mater Chem* **2010**, 20, 5251-5259.
31. Shokouhimehr, M.; Soehnlen, E. S.; Khitrin, A.; Basu, S.; Huang, S. P. D., *Inorg Chem Commun* **2010**, 13, 58-61.
32. Guari, Y.; Larionova, J.; Corti, M.; Lascialfari, A.; Marinone, M.; Poletti, G.; Molvinger, K.; Guerin, C., *Dalton Trans* **2008**, 3658-3660.
33. Chelebaeva, E.; Larionova, J.; Guari, Y.; Ferreira, R. A. S.; Carlos, L. D.; Trifonov, A. A.; Kalaivani, T.; Lascialfari, A.; Guerin, C.; Molvinger, K.; Datas, L.; Maynadier, M.; Gary-Bobo, M.; Garcia, M., *Nanoscale* **2011**, 3, 1200-1210.
34. Perrier, M.; Kenouche, S.; Long, J.; Thangavel, K.; Larionova, J.; Goze-Bac, C.; Lascialfari, A.; Mariani, M.; Baril, N.; Guerin, C.; Donnadieu, B.; Trifonov, A.; Guari, Y., *Inorg Chem* **2013**, 52, 13402-13414.
35. Dumont, M. F. Hoffman, H. A. Yoon, P. R., Conklin L. S., Saha, S. R. Paglione, J. P., Sze, R. W., Fernandes, R. *Bioconj. Chem.* **2014**, 25, 129-137.
36. Huang, S. D.; Li, Y.; Shokouhimehr M. Patent No WO 2011/106309 A2, 2011. Huang, S. D.; Khitrin, A. K.; Perera, V. S. Patent No WO 2012/108856 A1, 2012.
37. Tu, C. Q.; Ma, X. C.; Pantazis, P.; Kauzlarich, S. M.; Louie, A. Y., *J Am Chem Soc* **2010,** *132*, 2016-2023
38. Wadas, T. J.; Wong, E. H.; Weisman, G. R.; Anderson, C. J., *Chem Rev* **2010**, 110, 2858-2902.

